Buletin Ilmiah Sarjana Teknik Elektro
Vol. 8, No. 6, December 2026, pp. 1741-1758
ISSN: 2685-9572, DOI: 10.12928/biste.v8i6.17040

Energy-Based Modeling and GA-Optimized Sliding Mode Control of a Solar Roof Integrated Multifunctional EV Charger

Fajer M. Alelaj [1], **Birudala Venkatesh Reddy** [2], **M. S. Priyadarshini** [3], **T. Hemanth Kumar Chetty** [4], **Mohamed Metwally Mahmoud** [5, 6], **Alfian Ma'arif** [7], **Nagwa F. Ibrahim** [8]

[1] Water Research Center, Kuwait Institute for Scientific Research, Kuwait
[2] Department of Electrical and Electronics Engineering, Sri Venkateswara College of Engineering (Autonomous), Tirupati, 517507, Andhra Pradesh, India
[3] Department of Electrical and Electronics Engineering, K.S.R.M. College of Engineering (Autonomous), Kadapa 516005, Andhra Pradesh, India
[4] Power Grid Corporation of India Limited, Changlang 792120, Arunachal Pradesh, India
[5] ENET Centre, CEET, VSB—Technical University of Ostrava, Ostrava, 708 00, Czech Republic
[6] Department of Electrical Engineering, Faculty of Energy Engineering, Aswan University, Aswan, 81528, Egypt
[7] Department of Electrical Engineering, Universitas Ahmad Dahlan, Yogyakarta, Indonesia
[8] Electrical Department, Faculty of Technology and Education, Suez University, Suez 43527, Egypt;

ARTICLE INFORMATION

Article History:

Received 10 June 2026
Revised 21 September 2026
Accepted 16 December 2026

Keywords:

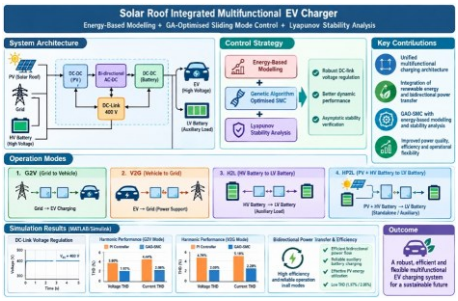
Electric Vehicle Charger;
Multifunctional On-Board Charger;
Vehicle-To-Grid;
Genetic Algorithm Optimized Sliding Mode Controller;
Green Energy Control

Corresponding authors:

M. S. Priyadarshini,
Department of Electrical and Electronics Engineering, K.S.R.M College of Engineering (Autonomous), Kadapa-516005, India
Email:
priyadarshini@ksrmce.ac.in

This work is open access under a Creative Commons Attribution-Share Alike 4.0

ABSTRACT



The growing penetration of RESs and the bidirectional power transfer capability in EV charging systems have led to the demand for multifunctional charging architectures with strong control and better power quality. However, the current research primarily concentrates on RE integration, multi-functional operation or advanced control strategies separately, while the combination of energy-based modelling with optimized non-linear control for multi-functional EV charging is still scarce. In this paper, energy-based modelling and control of a solar roof integrated multifunctional EV charger is presented using GAO-SMC. The proposed charger supports G2V, V2G, H2L and HP2L operation modes with the same power conversion architecture. The novelty of the proposed work is the integration of energy based mathematical model, GAO-SMC and Lyapunov stability analysis with the proposed unified multifunctional charging system. The energy-based model describes the power flow interactions between the utility grid, rooftop PV source, HVB and LVB through a common DC-link. The design of the proposed controller is used for robust DC-link voltage regulation and better dynamic performance. The Lyapunov stability analysis is used to verify the asymptotic stability of control strategy. The proposed system has been verified with MATLAB/Simulink simulations in all operation modes. Simulation results show the stable regulation of the DC link voltage at 400 V, the efficiency of the bidirectional power transfer, the reliability of the auxiliary battery charging and the effective exploitation of the rooftop PV energy. The proposed GAO-SMC reduces voltage THD from 3.80% to 1.97% and current THD from 4.44% to 2.08% in G2V mode, compared to a conventional PI controller. Likewise, the voltage THD is decreased from 4.76% to 2.05% in V2G mode, and the current THD is decreased from 5.18% to 2.28%. These results show that the proposed GAO-SMC has a significant improvement on voltage regulation, harmonic performance and operational flexibility, indicating its potential for future multifunctional EV charging applications.

Document Citation:

F. M. Alelaj, B. V. Reddy, M. S. Priyadarshini, T. H. K. Chetty, M. M. Mahmoud, A. Ma'arif, and N. F. Ibrahim, "Energy-Based Modeling and GA-Optimized Sliding Mode Control of a Solar Roof Integrated Multifunctional EV Charger," *Buletin Ilmiah Sarjana Teknik Elektro*, vol. 8, no. 6, pp. 1741-1758, 2026, DOI: 10.12928/biste.v8i6.17040.

1. INTRODUCTION

The rapid development of EVs has created a substantial demand for intelligent and efficient charging infrastructures. Electrification of transport is broadly seen as an effective way to minimise greenhouse gas emissions, strengthen energy security and foster sustainable mobility [1]-[3]. With penetration of EVs, onboard charging systems are required to perform battery charging while simultaneously supporting advanced EMS functions to improve efficacy of the EV and its interaction with the grid. Therefore, the development of multi-functional OBCs that can accomplish several power conversion tasks in one architecture has become an important research direction in modern EV technology [4]-[11]. Conventional OBCs are commonly designed for unidirectional battery charging and often require separate converters to supply low voltage auxiliary loads. These configurations increase system complexity, the number of converters, weight and overall cost. In order to overcome these limitations, multifunctional OBC architectures have been introduced to combine the charging and auxiliary power conversion functions into one system. These architectures improve converter utilisation and provide additional operating modes such as G2V, V2G and battery-to-load power transfer. The capability to support bidirectional energy flow is especially important for future smart-grid applications, where EVs can act as distributed energy storage resources and provide ancillary services to grid [12]-[16].

The integration of RESs to EV charging systems has gained significant interest in recent years. Among various RE technologies, PV systems are particularly attractive because they can directly use solar energy to charge EVs without additional fuel consumption. The solar roof integration offers a promising solution to improve energy autonomy of EV, reduce grid dependency, and improve sustainability of overall system [17]-[19]. Furthermore, the presence of rooftop PV generation can help LV-auxiliary loads and provide additional battery charging in suitable environmental conditions. However, the fluctuating nature of the solar irradiance and the load demands pose some additional challenges toward stable operation and satisfactory power quality of the multifunctional charging systems [20]-[23].

The dynamic performance of multifunctional OBCs is highly dependent on adopted control strategy. The most commonly used control method is the PI controller due to its simple implementation and low computational complexity [24]-[27]. However, PI controllers are susceptible to performance degradation when facing nonlinear operating conditions, parameter uncertainties and external disturbances. Such limitations can lead to slower transient response, larger steady-state errors and higher harmonic distortion. To overcome these limitations, SMC has been proposed as a robust nonlinear control technique which can provide fast dynamic response, strong disturbance rejection and improved system stability. The inherent robustness of SMC to parameter uncertainty has been widely investigated in applications of power electronic converters and EV ENSs [28]-[31]. However, performance of SMC strongly depends on appropriate selection of the controller parameters. If the parameters are not tuned properly, the control effort may be excessive and the dynamic performance degraded. In recent years, optimisation algorithms have been widely used for finding optimal controller settings in power electronic systems. Among these approaches, GAO has demonstrated a strong ability to solve nonlinear optimisation problems with evolutionary search mechanism [32]-[37]. GAO is used to systematically tune the controller parameters to improve transient response, voltage regulation and harmonic performance under different operating conditions. Therefore, the combination of GAO-SMC is a promising solution to improve the performances of the multifunctional EV charging systems.

A lot of research has been dedicated to the development of multifunctional OBCs, PV-assisted EV charging systems and sophisticated nonlinear control techniques. However, most of the reported works handle these aspects independently and little focus has been given to integrate RE utilisation, multifunctional charging capability and optimised robust control into a single charging architecture. Moreover, the comprehensive investigations in the existing literature are limited, covering all the four operating modes, i.e., G2V, V2G, H2L and HP2L together with systematic power quality improvement. Table 1 shows that the existing studies have addressed the multifunctional EV chargers from various aspects, such as RE integration, bidirectional charging capability and advanced control strategies. However, most of the reported works address only some aspects of the multifunctional operation and do not present a unified modelling framework for the analysis of the dynamic interactions between the utility grid, rooftop PV source, HVB, LVB and the common DC-link. In addition, systematic validation of all four modes of operation, systematic stability checking and quantitative PQ assessment are still limited. These limitations motivate the development of a unified modelling and control framework for multi-functional EV charging systems. In order to overcome these limitations, this paper proposes an energy-based modelling and control framework for a solar roof integrated multifunctional EV charger using a GAO-SMC. It is developed to characterised the dynamics of power flow through the common DC-link. The controller parameters are optimally tuned using a GAO to achieve robust DC-link voltage regulation and improved dynamic performance. Lyapunov stability analysis is performed to prove the asymptotic stability of proposed control scheme. The proposed multifunctional charging architecture can

support G2V, V2G, H2L and HP2L operation modes and is verified by MATLAB/Simulink simulations. Performance is quantified and contrasted with a conventional PI controller in terms of voltage regulation, harmonic distortion and general operational performance.

This paper is arranged next as Section 2 describing proposed multifunctional EV charger architecture, its operating principles and energy flow analysis. Section 3 presenting energy-based mathematical modelling, the design of GAO-SMC and Lyapunov stability analysis. The simulation results of G2V, V2G, H2L and HP2L modes are presented in Section 4, along with the comparison of performance. Finally, Section 5 concludes the paper.

Table 1. Comparison of existing multi-functional EV charging systems

Ref.	System Configuration	PV Integration	Control Method	Supported Modes	Limitation
[1]	Multifunctional OBC with APD	No	PI	G2V, V2G, H2L	No renewable energy integration
[16]	Renewable-assisted multifunctional charger	Yes	SMC	G2V, V2G	Limited power quality analysis
[38]	Integrated onboard charger	No	PI	G2V, V2G	Limited dynamic response
[39]	Multifunctional EV charger	No	PI	G2V, V2G, H2L	Higher harmonic distortion
[40]	PV-Assisted EV Charger	Yes	PI	G2V	No bidirectional power transfer
[41]	Solar roof integrated OBC	Yes	PI	G2V, V2G, H2L, HP2L	Limited control robustness
[42]	Bidirectional EV charger	No	SMC	G2V, V2G	No auxiliary battery support
Proposed Work	Solar roof integrated multifunctional EV charger	Yes	GAO-SMC	G2V, V2G, H2L, HP2L	Enhanced voltage regulation and reduced THD

2. PROPOSED MULTIFUNCTIONAL EV CHARGER

The proposed multi-functional EV charger combines a common power conversion architecture consisting of a rooftop PV source, a HVB and an LVB. The system allows G2V, V2G, H2L and HP2L operation modes to enable bidirectional power transfer and utilisation of RE. The proposed charger uses a shared converter structure to improve power utilisation, reduce system complexity, and improve operational flexibility for electric vehicle applications [43]-[46].

2.1. Architecture of System

Figure 1 shows architecture of the proposed multifunctional EV charger. The system comprises a grid-side AC-DC converter, a DC-link capacitor, a bidirectional DC-DC converter connected to HVB, a LV DC-DC converter and a rooftop PV source. Grid-side converter is utilised for power factor correction and regulation of DC-link voltage during the charging and discharging operations. The bidirectional DC-DC converter facilitates energy transfer between the DC-link and HVB, while the LV converter provides power to the LVB and auxiliary EV loads [47][48]. The charger architecture integrates the rooftop PV source to improve utilisation of RE and reduce dependence on utility grid [49][50]. Depending on the operating condition, the PV source can either directly feed power into the charging process of LVB or operate in coordination with HVB. Thus, the proposed configuration allows an efficient management of the energy while minimising the number of dedicated power conversion stages [51]-[53].

2.2. Operation Modes

Figure 2 illustrates the operating modes of the proposed OBC for a plug-in EV under different parking and driving conditions. During daytime parking (Figure 2a), when solar generation is available, the EV can operate in mode 1 (G2V) for charging or mode 2 (V2G) for power transfer through the AC–DC and DC–DC converters. In addition, mode 4 (P2L-standalone) enables the battery to supply a local load through the LDC converter, allowing standalone power delivery. During nighttime or indoor parking (Figure 2b), solar generation is unavailable, and the OBC supports bidirectional grid interaction through modes 1 and 2, while mode 3 (H2L) allows the battery to supply household loads through the LDC converter. The indicated no simultaneous condition emphasizes that G2V and V2G operation are mutually exclusive. During driving (Figure 2c), the EV is electrically isolated from the grid, while the OBC and LDC paths support auxiliary power-transfer functions. In this condition, mode 3 (H2L) provides power to household or auxiliary loads, whereas mode 4 (HP2L/P2L-standalone) supports standalone loads, with the associated paths incorporating

MPPT where applicable. Overall, Figure 2 demonstrates the multifunctional capability of the proposed OBC to accommodate grid charging, grid support, household-load supply, and standalone power delivery according to the vehicle's operating condition.

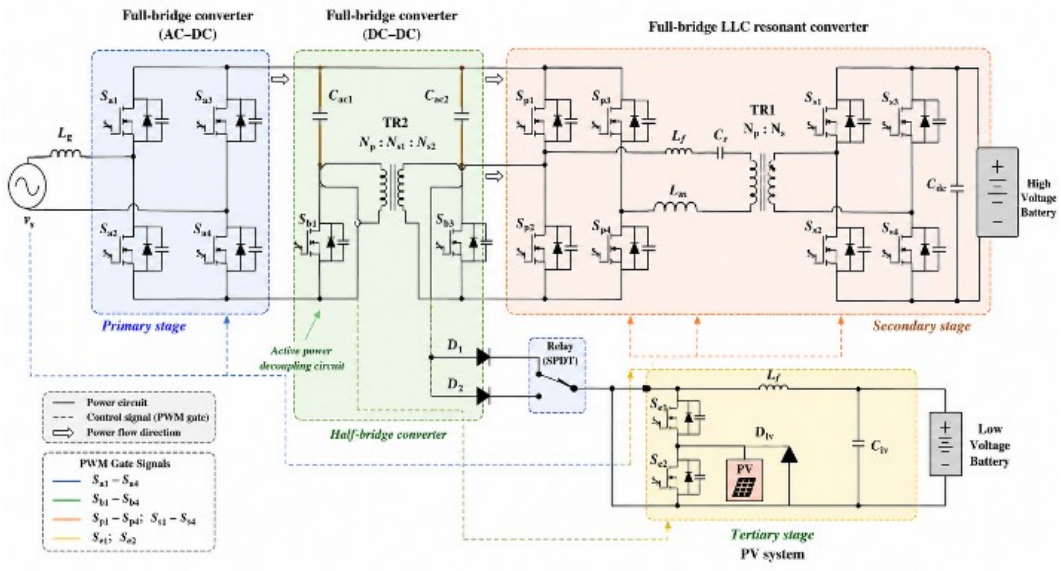


Figure 1. Proposed multifunctional EV charger architecture

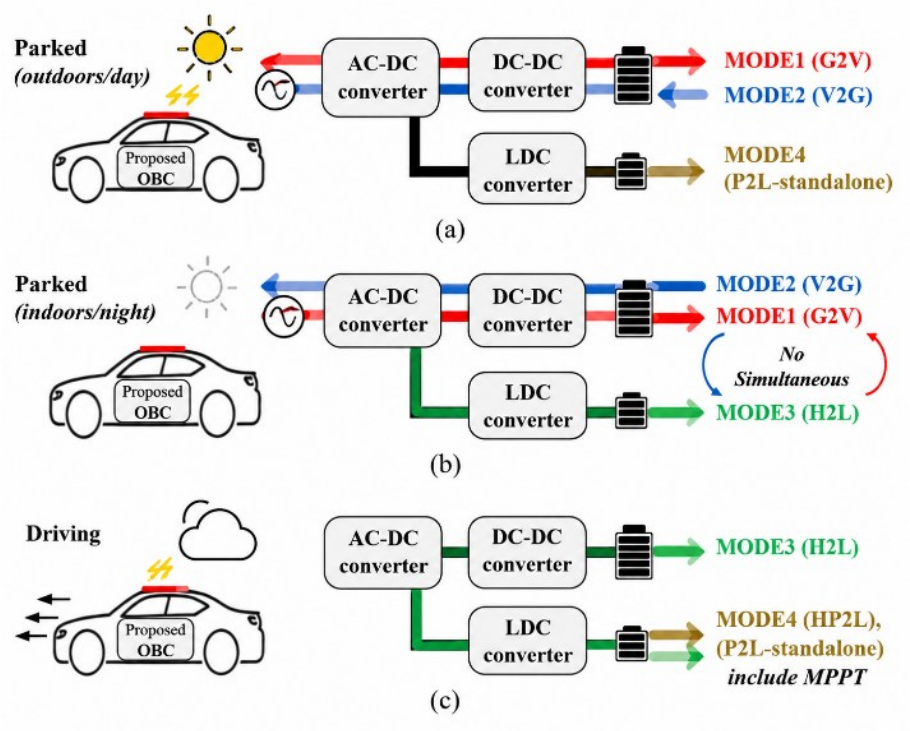


Figure 2. Power flow in G2V, V2G, H2L and HP2L operation modes

2.2.1. G2V Mode

In G2V mode, OBCs transfers electrical energy from utility grid to high-voltage battery. The grid-side converter controls DC-link voltage and achieves sinusoidal grid current operation with high power factor. The bidirectional DC–DC converter works in charging mode and supplies necessary charging current to the HVB. This mode is the traditional battery charging operation of the EV [54]-[56].

2.2.2. V2G Mode

In a V2G mode, HVB supplies its stored energy back to utility grid. The bidirectional converter provides power from battery to DC-link and the grid side converter injects current into the grid [57]-[60]. This mode of operation enables EV battery to be a distributed energy storage resource to support grid demand and smart-grid applications.

2.2.3. H2L Mode

In H2L mode, HVB supplies power to LVB via LV-DC–DC converter. It is used to keep auxiliary battery charged and power LV-EV loads when external charging sources are not available [61]-[63]. The operation guarantees the uninterrupted provision of auxiliary power in the EV.

2.2.4. HP2L Mode

In the HP2L mode, the rooftop PV source and the HVB provide power to charge LVB. PV source provides RE when there is solar irradiation, thus reducing the energy drawn from the HVB [64]-[66]. This operating mode increases the utilization of RESs and overall efficiency of charging system.

2.2.5. Mode Transition Strategy

The operating mode of proposed multifunctional EV charger is selected based on availability of the utility grid, rooftop PV source, battery state-of-charge and charging demands. Such operating conditions are monitored continuously by a supervisory control unit which produces the corresponding mode command signal [67]-[69]. The appropriate converter switches and control loops are activated according to selected mode, thereby establishing necessary power flow path through common DC link. In this work, dynamic performance of proposed controller is evaluated by considering a transition from the G2V mode to the V2G mode. The transition is accomplished by the change of mode command signal at the specified switching instant which changes reference current direction thereby reversing power flow between the utility grid and the HVB.

2.3. Energy Flow Analysis

The proposed multifunctional EV charger provides bidirectional power exchange between utility grid, rooftop PV source, HVB and LVB through a common DC-link. Selected operating mode changes the power flow direction and regulation of DC-link voltage [70].
Power on grid side is [70]:

$$\mathbf{P_g} = \mathbf{V_g} \times \mathbf{I_g} \tag{1}$$

where V_g and I_g denote grid voltage and grid current respectively.
Similarly, the power of the photovoltaic source is expressed as [70]:

$$\mathbf{P_{PV_}} = \mathbf{V_{PV}} \times \mathbf{I_{PV}} \tag{2}$$

where V_{PV} and I_{PV} denote PV voltage and current, respectively.
The power transferred from HVB to LVB can be written as [70]:

$$\mathbf{P_{HV}} = \mathbf{V_{HV}} \times \mathbf{I_{HV}} \tag{3}$$

and

$$\mathbf{P_{LV}} = \mathbf{V_{LV}} \times \mathbf{I_{LV}} \tag{4}$$

DC-link capacitor is an intermediate energy storage element to facilitate power balancing between different energy sources and loads. The energy stored in dc-link capacitor is expressed as [70]:

$$\mathbf{E_{dc}} = \frac{\mathbf{1}}{\mathbf{2}}\mathbf{C_{dc}} \times (\mathbf{V_{dc}})^{\mathbf{2}} \tag{5}$$

where C_{dc} and V_{dc} denote DC-link capacitance and voltage, respectively.

During G2V operation the HV battery is charged from the utility grid power. In V2G mode the energy stored in HVB is sent back to utility grid. In H2L mode, HVB supplies power for charging LVB. In HP2L mode, the HVB and the rooftop PV source both contribute to charging the LVB. Hence, the DC-link serves as a common energy exchange interface to all operating modes and its voltage must be tightly controlled for a stable operation of the system. The energy flow relationships developed in this section form the basis of the mathematical modelling and the controller design presented in the next section.

3. MATHEMATICAL MODELING AND GAO-SMC

This section presents the mathematical model and controller design for the proposed multifunctional EV charger. According to the energy flow relations obtained in Section 2, an energy-based mathematical model is established with the common DC-link as the energy coupling element. The derived model is used for the design of the proposed controller, and then, the parameters are optimised by the GAO, Lyapunov stability analysis is performed to show the stability of the closed-loop system.

3.1. Dynamic Energy Modelling

The dynamic behaviour of proposed multifunctional EV charger is governed by energy stored in common DC-link capacitor, which acts as energy exchange interface among utility grid, rooftop PV source, HVB and LVB. Therefore, an energy-based modelling approach is adopted to develop a mathematical model of the system dynamics. According to principle of conservation of energy, rate of change of stored energy is equal to difference between total input power and total output power [71]. Then, the power balance equation of the proposed charger can be written as:

$$\frac{dE_{dc}}{dt} = P_g + P_{PV} - P_{HV} - P_{LV} \tag{6}$$

where P_g denote power supplied from utility grid, P_{PV} is PV power, P_{HV} is the power exchanged with the HVB, and P_{LV} is the power supplied to LVB.
Substituting the expression for stored energy into power balance equation gives:

$$\frac{d}{dt}\left(\frac{1}{2}C_{dc} \times (V_{dc})^2\right) = P_g + P_{PV} - P_{HV} - P_{LV} \tag{7}$$

which may be reduced further to:

$$C_{dc}V_{dc}\frac{dV_{dc}}{dt} = P_g + P_{PV} - P_{HV} - P_{LV} \tag{8}$$

Therefore, dynamic behaviour of DC-link voltage can be expressed by

$$\frac{dV_{dc}}{dt} = \frac{P_g+P_{PV}-P_{HV}-P_{LV}}{C_{dc}V_{dc}} \tag{9}$$

The equation shows that DC-link voltage is controlled by instantaneous power imbalance between the grid, the photovoltaic source and battery subsystems. During G2V operation, the grid provides charging power to the high voltage battery. In V2G mode, power moves from HVB to utility grid. During H2L operation, HVB is used to charge LVB while during HP2L mode, LVB charging process is assisted by PV source and HVB [72]. Therefore, a good regulation of DC-link voltage is necessary for a stable operation in all modes of operation. Energy model developed in this section forms basis for design of proposed GAO-SMC.

3.2. Sliding Surface Design

The main control objective is to regulate the DC-link voltage around its reference value in the different operation modes [73]. The purpose of the controller is to drive the system trajectory onto sliding surface and to ensure stable operation in charging and discharging processes.
Thus, the DC link voltage error is expressed as:

$$e(t) = V_{dc}^* - V_{dc} \tag{10}$$

where, V_{dc}^* is the reference DC link voltage and V_{dc} is measured DC-link voltage.
A first order sliding surface is chosen to guarantee a fast convergence and a robust voltage regulation, which is defined as:

$$s(t) = \lambda\, e(t) + \frac{de(t)}{dt} \tag{11}$$

where $\lambda > 0$ is sliding surface gain that determines the convergence rate of the controller.

3.3. Control Law

SMC input consists of an equivalent control component and a switching control component. The equivalent control maintains the system trajectory on the sliding surface, whereas the switching control drives the system states towards the sliding manifold. Accordingly, control law is expressed as [74][75]:

$$u = u_{eq} + u_{sw} \tag{12}$$

where u_{eq} is equivalent control action that keeps system trajectory on sliding surface, and u_{sw} is discontinuous control part that drives system states towards sliding manifold. For ideal sliding motion, the time derivative of sliding surface is enforced to be zero.

$$\dot{s} = 0 \tag{13}$$

which guarantees that once system trajectory reaches sliding surface, it remains on it. Substituting DC-link dynamic model (9) into derivative of sliding surface and applying the condition (13), the equivalent control action can be formulated based on the sliding surface dynamics and the energy-based model of the proposed multifunctional EV charger.

$$u_{eq} = f(x)^{-1}(\dot{V}_{dc}^{ref} + \lambda e) \tag{14}$$

where $f(x)$ is the nonlinear dynamics of proposed charger representing the nonlinear dynamics obtained from energy-based DC-link model, $\dot{V}_{dc}^{ref}$ is the derivative of reference DC-link voltage, λ is sliding surface parameter and e is DC-link voltage error.

The equivalent control component provides the nominal control action needed for DC-link voltage regulation and maintains system trajectory on the sliding manifold under ideal operating conditions. The switching control element is written as:

$$u_{sw} = -ksat\left(\frac{s}{\emptyset}\right) \tag{15}$$

where k is a positive switching gain, $\emptyset$ is boundary layer thickness and sat is saturation function which is defined as:

$$sat\left(\frac{s}{\emptyset}\right) = \begin{cases} 1, & s > \emptyset \\ \frac{s}{\emptyset}, & |s| \le \emptyset \\ -1, & s < \emptyset \end{cases} \tag{16}$$

Then overall control law is:

$$u = u_{eq} - ksat\left(\frac{s}{\emptyset}\right) \tag{17}$$

In switching control component, a boundary-layer saturation function is used to eliminate chattering phenomenon which is usually caused by the ideal sign function. Consequently, abrupt switching of the control input is avoided, thereby protecting the converter switches and reducing electromagnetic interference. The saturation function is used to smooth the control action close to the sliding surface and hence reduces the high frequency switching, stress on the converter and electromagnetic interference while maintaining the robust features of the sliding mode controller. Thus, proposed controller provides a good trade-off between dynamic performance and practical implementation requirements. The switching gain influences the rate of convergence of the system states to sliding surface, and improves robustness against parameter uncertainties and external disturbances. Hence, an optimal trade-off between the dynamic performance and the control effort can be achieved by properly tuning the controller parameters. In this work, the parameters of the controller are optimally tuned using GAO as described in the next sub-section.

The implementation structure of proposed GAO-SMC is shown in Figure 3. The DC-link voltage error and its derivative build the sliding surface. The control signal generated drives the power conversion stages to keep DC-link voltage equal to reference value. The resulting GAO-SMC provides robust DC-link voltage regulation under different operating modes while improving transient response and harmonic performance.

3.4. GAO Method

The performance of SMC depends heavily on the choice of controller parameters. Improper parameter selection may result in large overshoot, slow convergence speed and poor voltage regulation performance [65], [76]. Therefore, optimal controller parameters of the proposed SMC are obtained by utilizing a GAO. The GAO settings used in work are given in Table 2, including population size, crossover rate, mutation rate and number of generations. The GAO parameter values listed in Table 2 were chosen based on preliminary simulation studies to balance between optimization accuracy and computational effort. A population size of 50

and 100 generations are enough to get enough search capability and convergence while the crossover and mutation rates maintain a suitable balance between global exploration and local exploitation during the optimization process. The controller parameters are represented in the form of chromosomes during the optimization process and are evaluated by a fitness function based on DC-link voltage regulation error. The objective function is given as:

$$J = \int_0^T |e(t)|\, dt \tag{18}$$

where J is the fitness value, $e(t)$ is DC-link voltage error and T is the simulation time.

The optimization objective is to minimize the voltage tracking error with fast dynamic response and less steady-state error. A GAO starts with an initial population of candidate solutions. New generations of controller parameters are produced and evaluated iteratively by selection, crossover and mutation operations. The optimization process continues until the stopping criterion is met and the optimal controller parameters are obtained and used in the proposed GAO-SMC [77]. Figure 4 shows the overall optimization procedure.

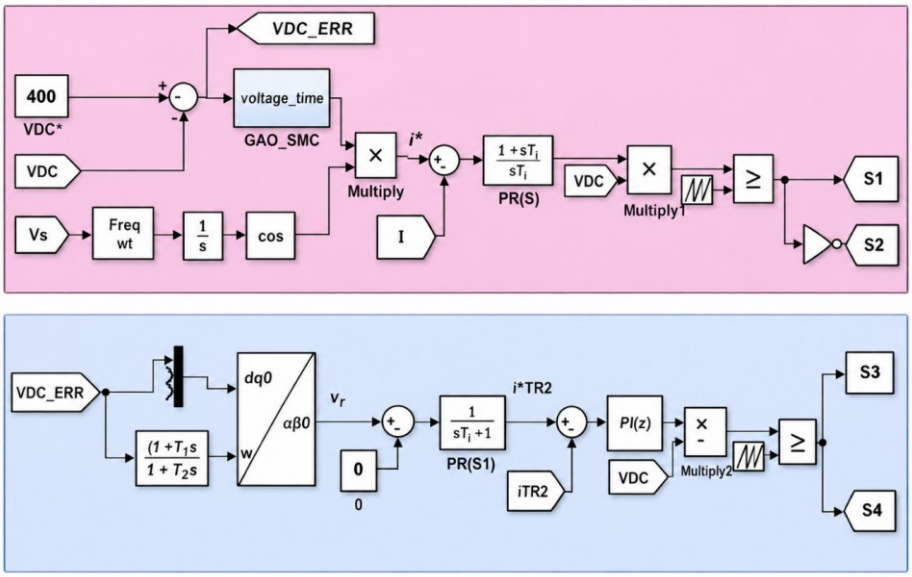


Figure 3 Block diagram of proposed GAO-SMC controller

Table 2. GAO parameters of controller

Parameter	Value
Population Size	50
Number of Generations	100
Crossover Rate	0.8
Mutation Rate	0.05
Fitness Function	IAE

3.5. Lyapunov Stability Analysis

The asymptotic stability of the proposed GAO-SMC is analysed using Lyapunov's direct method. The objective is to demonstrate that the DC-link voltage tracking error converges to zero while ensuring closed-loop stability under different operating modes. We select a candidate Lyapunov function as:

$$V(s) = \frac{1}{2}s^2 \tag{19}$$

where s represents the sliding surface.

The selected Lyapunov function is positive definite because $V(s) > 0$ for all $s \neq 0$ and $V(s) = 0$ only if $s = 0$. Let's differentiate the Lyapunov function with respect to time:

$$\dot{V}(s) = s\dot{s} \tag{20}$$

The sliding surface dynamics are given by the sliding mode reaching condition as:

$$\dot{s} = -ksign(s) \tag{21}$$

where $k > 0$ is a switching gain. Substituting the reaching law into the Lyapunov derivative we have:

$$\dot{V}(s) = s(-ksign(s)) \tag{22}$$

which reduces to:

$$\dot{V}(s) = -k|s| \tag{23}$$

Since $k > 0$, derivative of Lyapunov function is:

$$\dot{V}(s) < 0, \quad \forall s \neq 0 \tag{24}$$

Hence the Lyapunov function decreases monotonically with time and the system trajectories converge to the sliding surface. Since the switching gain satisfies $k > 0$, the Lyapunov function derivative remains negative definite whenever the system trajectory is away from the sliding surface. Consequently, the sliding variable converges asymptotically to zero, ensuring asymptotic stability of the closed-loop DC-link voltage regulation system.

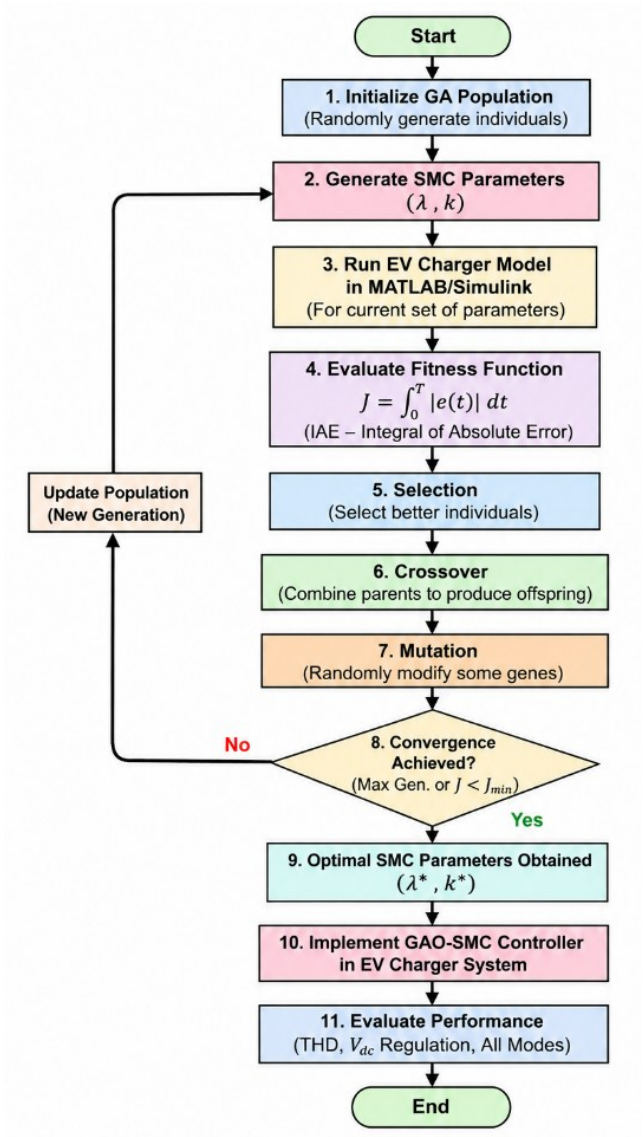


Figure 4. Flowchart of proposed GAO-SMC technique

4. RESULTS AND DISCUSSION

The performance of proposed solar roof integrated multifunctional EV charger was modelled and evaluated in MATLAB/Simulink environment to validate performance under different operating conditions. Proposed GAO-SMC was verified for its effectiveness in the DC-link voltage regulation, bidirectional power transfer capability, PV energy utilisation and harmonic performance. Simulation parameters used in study are summarised in Table 3. The charger performance was assessed in the G2V, V2G, H2L and HP2L operation modes. Next subsections are devoted to presenting and discussing simulation results.

Table 3. Simulation parameters of the proposed system

Parameter	Symbol	Value
Grid Voltage	V_g	230 V
Grid Frequency	f_g	50 Hz
DC Link Voltage	V_{dc}	400 V
High-Voltage Battery Voltage	V_{HVB}	400 V
Low-Voltage Battery Voltage	V_{LVB}	12 V
PV Rated Power	P_{PV}	180 W
DC-Link Capacitor	C_{dc}	2200 µF
Switching Frequency	f_s	50 kHz
Simulation Time	T	5 s

4.1. G2V Operation

The performance of suggested multifunctional EV charger in the G2V mode is shown in Figure 5. The DC link voltage is kept stably regulated, while electrical energy is transferred from utility grid to HVB in this operating mode. Figure 5(a) shows grid voltage and grid current wave forms. The grid current is observed to be almost in phase with grid voltage, which indicates near unity power factor operation and effective power transfer from the utility grid to the battery charging system. Figure 5(b) shows DC-link voltage response with the proposed GAO-SMC. The DC-link voltage converges quickly to its reference value of 400 V with small overshoot and fast settling characteristics. The obtained response shows ability of proposed controller to provide stable operation in the presence of transient conditions during the charging process. The charging characteristics of the HVB are shown in Figure 5(c) and Figure 5(d). The charging current converges to the desired reference and battery voltage approaches to its rated value of operation.

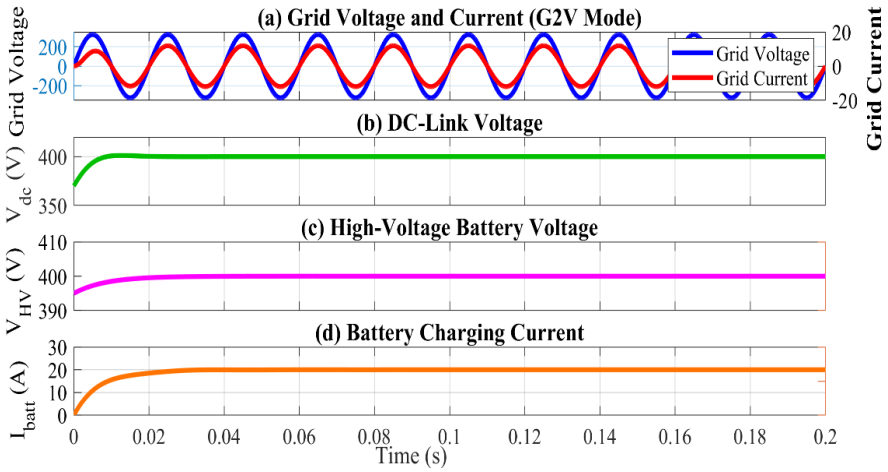


Figure 5. Simulation results of the G2V mode: (a) grid voltage and current, (b) DC link voltage regulation, (c) HVB voltage, and (d) battery charging current

4.2. V2G Operation

The performance of proposed multifunctional EV charger in V2G mode is presented in Figure 6. In this mode, the stored energy in HVB can be transferred back to utility grid, i.e., the power flow is bidirectional and energy management on the grid side can be achieved. Figure 6(a) shows waveforms of grid voltage and grid current. The grid current can be seen to be phase shifted with respect to the grid voltage which indicates power injection from battery to utility grid. The response of DC-link voltage under V2G operation is shown in Figure 6(b). Although direction of power flow is reversed, proposed GAO-SMC can control DC-link voltage to the reference value of 400 V with fast transient response and negligible steady-state error. The steady DC-link

voltage shows robustness of controller to different operating conditions and power transfer requirements. Figure 6(c) and Figure 6(d) show the HVB voltage and the battery current characteristics, respectively. When V2G operation is performed, battery is discharging to grid and battery voltage gradually decreases. The battery current is negative, which means battery operates in the discharge mode. The smooth discharge profile and stable voltage response confirm the capability of the proposed charger to support controlled energy export and system stability.

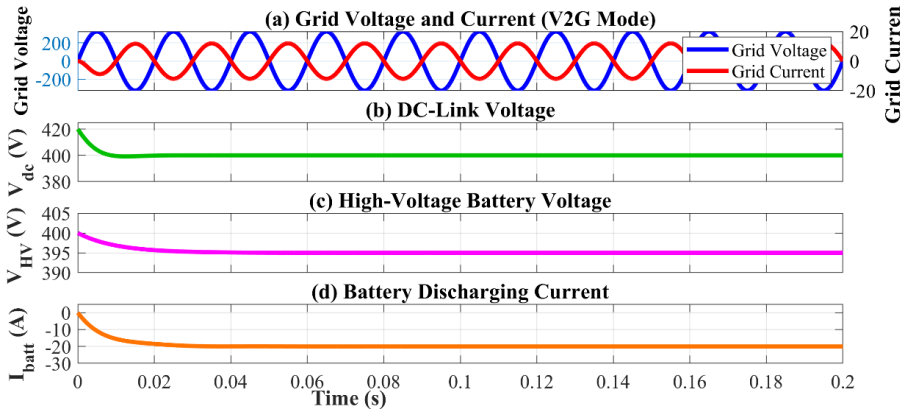


Figure 6. Simulation results of the V2G mode: (a) grid voltage and current, (b) DC-link voltage regulation, (c) HVB voltage, and (d) battery charging current

4.3. H2L Operation

The H2L operating mode is used to charge auxiliary LVB using energy stored in HVB. The simulation results corresponding to this are shown in Figure 7. In this mode, the power is transferred internally within the vehicle without any support from either the utility grid or the PV source. This function allows to eliminate a dedicated auxiliary battery charger and improves the overall utilisation of the existing power conversion stages.

Figure 7(a) shows HVB voltage during H2L operation. During the energy delivery to the LVB, one can observe a small decrease in the battery voltage. The corresponding HVB current is shown in Figure 7(b), where a negative current denotes battery discharge operation. The smooth current profile indicates a controlled power transfer and an efficient operation of the tertiary conversion stage. The response of DC-link voltage is shown in Figure 7(c). It can be seen that proposed GAO-SMC keeps DC-link voltage close to reference value of 400 V under the change of the power flow conditions. The fast settling and the small steady state error shows robustness of controller to keep system operating in a stable manner. Figure 7(d) shows the LVB charging voltage. The voltage rises slowly to the desired level. This shows that the auxiliary battery has been successfully charged. The results show that the proposed multifunctional charger has the capability of an efficient H2L operation with steady regulation of DC-link voltage and reliable auxiliary battery charge performance.

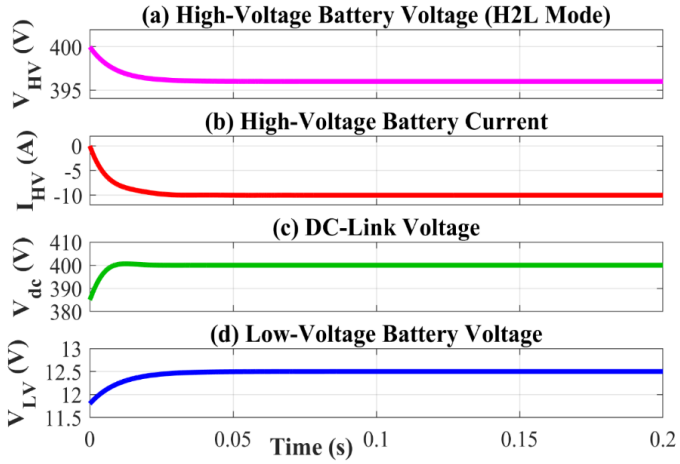


Figure 7. Simulation results of the H2L mode: (a) high-voltage battery voltage, (b) high-voltage battery current, (c) DC-link voltage regulation, and (d) low-voltage battery charging voltage

4.4. HP2L Operation

The HP2L operating mode demonstrates the performance of the proposed charger to harness energy from rooftop PV energy to charge auxiliary battery. The results of the corresponding simulation are presented in Figure 8. In this mode, the PV source contributes to charging the LVB, which reduces the energy demand on HVB and increases the use of RE by the EV. The PV voltage response during operation of the HP2L is shown in Figure 8(a). The PV voltage quickly arrives at the rated operating value and stays stable during the whole charging process. The corresponding PV power is shown in Figure 8(b), in which the generated power gradually increases and reaches rated value. This demonstrates effective use of the rooftop PV source to support the auxiliary charging process. The response of the DC-link voltage is shown in Figure 8(c). The proposed GAO-SMC is able to keep DC-link voltage around reference value of 400 V with very low oscillations and fast settling characteristics even when the PV source and the HVB are connected simultaneously. The constant DC-link voltage shows the robustness of controller for case of multi-source power transfer. The charging characteristics of LVB are presented in Figure 8(d). The battery voltage rises steadily and reaches the required charge level and power transfer is efficient from the PV source and HVB. Compared with the H2L mode, the HP2L mode allows partial utilization of RE, thus reducing dependence on HVB and improving overall energy efficiency of charging system. The results demonstrate the effectiveness of the proposed charger to integrate the rooftop PV energy, while maintaining stable operation of the system and reliable LVB charging performance.

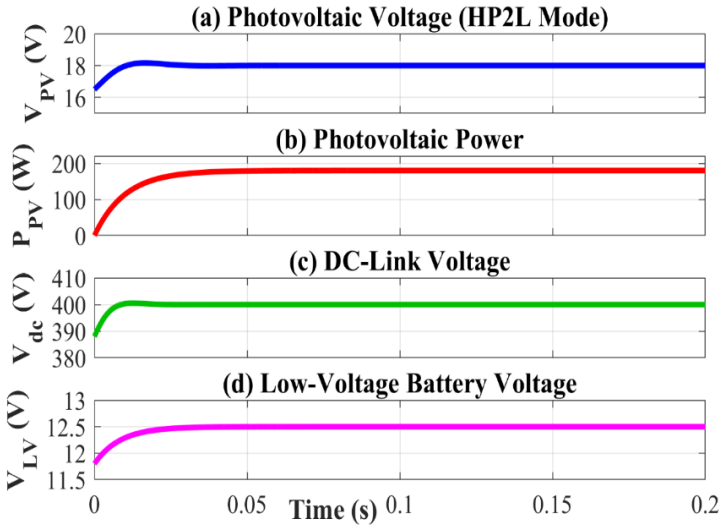


Figure 8. Simulation results of the HP2L mode: (a) photovoltaic voltage, (b) photovoltaic power, (c) DC-link voltage regulation, and (d) low-voltage battery charging voltage

4.5. Stability and Mode Transition Analysis

The stability of the proposed GAO-SMC is verified using both theoretical analysis and simulation studies. In Section 3.5 it is shown that the Lyapunov stability analysis shows that derivative of selected Lyapunov function is negative definite, which guarantees convergence of system trajectories to sliding surface. As a consequence, the DC-link voltage regulation error asymptotically converges to zero to ensure a stable closed loop operation. The simulation results of Figure 5 to Figure 8 are further confirming stability of proposed controller in all operating modes. In G2V mode, DC-link voltage converges quickly to reference value of 400 V during battery charging without sustained oscillations. Similarly, stable voltage regulation is also achieved during V2G operation despite the reversed power flow direction from high-voltage battery to utility grid. The tight regulation of DC-link voltage during power transfer to low-voltage battery in H2L and HP2L modes is demonstrated. Moreover, the rooftop photovoltaic source integration in HP2L mode does not cause any instability or unwanted oscillatory behaviour. The smooth voltage and current responses obtained in all operating modes demonstrate the robustness of the proposed controller under various power flow conditions.

To further assess dynamic performance of proposed controller, a mode transition study based on the supervisory mode-selection strategy presented in Section 2.2.5 was conducted by switching the operating mode from G2V to V2G at t = 2s. The results are shown in Figure 9. Before transition, power is shifted from utility grid to high voltage battery. After the transition instant, power flow direction is reversed and energy is fed back

to utility grid from high voltage battery. It can be seen that the grid current reverses its direction immediately after the mode transition, where the battery current changes from charging to discharge operation. The proposed GAO-SMC is able to keep DC-link voltage around its reference value of 400 V with a small transient deviation and fast recovery even though the operating conditions are changed abruptly. The obtained results show the proposed controller can handle the transition of the operating mode without instability, overshoot or sustained oscillations. Therefore, the proposed GAO-SMC provides a stable regulation of DC-link voltage, a robust dynamic response, and a reliable operation under both steady-state and transient operating conditions, which is suitable for multifunctional EV charging applications with bidirectional power transfer and renewable energy integration.

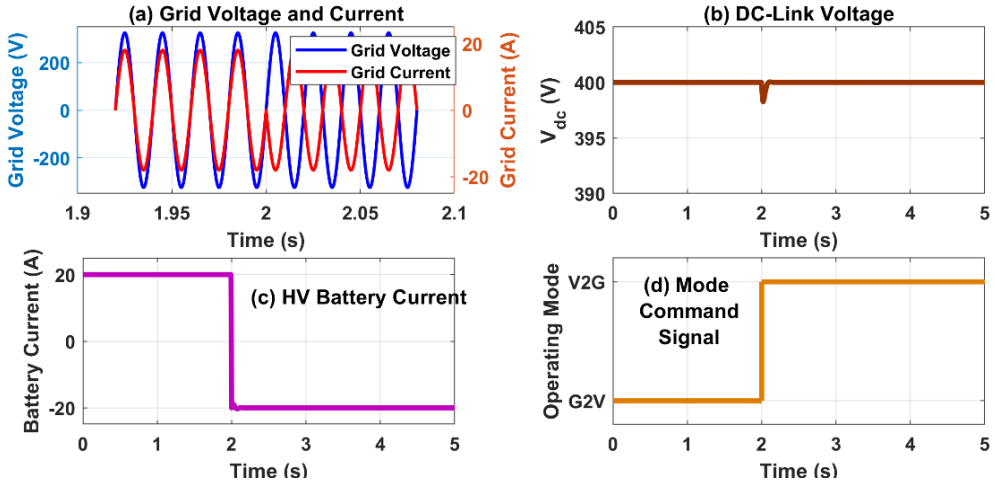


Figure 9. Performance of the proposed V2G/G2V system: (a) grid voltage and grid current during the mode transition, (b) DC-link voltage, (c) HV battery current, and (d) operating mode command signal

4.6. Harmonic Analysis

The harmonic performance of proposed charger was investigated by comparing THD obtained using the conventional PI controller and the proposed GAO-SMC. The corresponding results are summarised in Table 4. Harmonic distortion is an important performance indicator in EV charging systems as excessive voltage and current harmonics can negatively affect power quality, converter efficiency and grid compatibility. The proposed GAO-SMC is shown in Table 4 to greatly reduce the voltage and current THD in both G2V and V2G operation modes. In G2V mode, voltage THD is reduced from 3.80% to 1.97%, and the current THD is reduced from 4.44% to 2.08%. Similarly, in V2G mode, the voltage THD is reduced from 4.76% to 2.05% and the current THD is reduced from 5.18% to 2.28%. The results indicate excellent performance of proposed controller in controlling the operation of the converter and reducing the harmonic contents. The reduction of the harmonic distortion is due to the proper tuning of the controller parameters by the GAO and the intrinsic robustness of the SMC strategy. The improved DC-link voltage regulation leads to a smoother converter switching behaviour and better power transfer characteristics, which in turn reduces harmonic content in the voltage and current waveforms.

Table 4 Comparison of THD between PI and GAO-SMC controllers.

Parameter	PI (%)	GAO-SMC (%)
Voltage THD (G2V)	3.80	1.97
Current THD (G2V)	4.44	2.08
Voltage THD (V2G)	4.76	2.05
Current THD (V2G)	5.18	2.28

5. CONCLUSIONS

This paper presented the modelling and control of solar roof integrated multifunctional EV charger using GAO-SMC. An energy based mathematical model was developed to describe the interactions of power flow between the utility grid, PV source, HVB and LVB via a common DC-link. Furthermore, the Lyapunov stability analysis was carried out to verify asymptotic stability of proposed control strategy. The proposed charger is validated in MATLAB/Simulink for G2V, V2G, H2L and HP2L modes of operation. The simulation results demonstrated stable regulation of the 400 V DC-link voltage at all operating conditions, with bidirectional

power flow, auxiliary battery charging and PV energy utilization in one single charging topology. The harmonic performance of proposed controller was assessed and compared with a conventional PI controller. For the G2V mode, the THD of the voltage was reduced from 3.80% to 1.97% and that of the current was reduced from 4.44% to 2.08%. Similarly, the voltage THD was reduced from 4.76% to 2.05% and the current THD was decreased from 5.18% to 2.28% in the V2G mode. These results confirm the superior voltage regulation capability and harmonic suppression performance of the proposed GAO-SMC. Overall, proposed charger successfully integrates EV charging, V2G, auxiliary battery management, and solar roof energy harvesting in one platform. The developed energy-based model, Lyapunov stability verification and improved harmonic performance signify the suitability of the proposed approach to next-generation multifunctional EV charging applications.

List of abbreviations

THD	:	Total harmonic distortion
GAO-SMC	:	Genetic algorithm optimised sliding mode controller
RESs	:	Renewable energy sources
HP2L	:	High-voltage battery and photovoltaic-to-low-voltage battery
H2L	:	High-voltage battery to low voltage battery
EMSs	:	Energy management systems
G2V	:	Grid to Vehicle
V2G	:	Vehicle-to-Grid
PQ	:	Power quality
H\LVB	:	high\low-voltage battery
EVs	:	electric vehicles
OBCs	:	on-board chargers

DECLARATION

Author Contribution

All authors contributed equally to the main contributor to this paper. All authors read and approved the final paper.

Acknowledgment

This article has been produced with the financial support of the European Union under the REFRESH—Research Excellence For REgion Sustainability and High-tech Industries project number CZ.10.03.01/00/22_003/0000048 via the Operational Programme Just Transition.

Conflicts of Interest

The authors declare no conflict of interest.

REFERENCES

[1] J. Lee and J. Won, "Multifunctional onboard charger for electric vehicles integrating a low-voltage DC–DC converter and solar roof," *IEEE J. Emerg. Sel. Top. Power Electron.*, vol. 12, no. 1, pp. 283–294, 2024, https://doi.org/10.1109/JESTPE.2023.3309974.

[2] M. Miloudi *et al.*, "Comprehensive experimental performance investigation of conducted electromagnetic interference in split-phase induction motors: Common-mode," *J. Low Freq. Noise Vib. Act. Control*, vol. 0, no. 0, pp. 1–20, 2026, https://doi.org/10.1177/14613484251411703.

[3] M. F. Elnaggar, M. M. Mahmoud, A. Benselama, and S. N. Fahmy, "Crayfish optimization–tuned FOPID controller for frequency stability and energy management in electric vehicle-assisted renewable microgrids," *Int. J. Robot. Control Syst.*, vol. 6, no. 3, pp. 1889–1912, 2026, https://doi.org/10.31763/ijrcs.v6i3.2672.

[4] B. Noll *et al.*, "Battery-electric passenger vehicles will be cost-effective across Africa well before 2040," *Nat. Energy*, vol. 11, no. 2, pp. 284–298, 2026, https://doi.org/10.1038/s41560-025-01955-x.

[5] M. F. Elnaggar, M. M. Mahmoud, and A. Benselama, "Robust frequency regulation in PV – electric vehicle integrated microgrids via hybrid crayfish optimization and balloon effect adaptive control," *Int. J. Robot. Control Syst.*, vol. 6, no. 3, pp. 2003–2024, 2026, https://doi.org/10.31763/ijrcs.v6i3.2673.

[6] M. F. Elnaggar, I. M. Elzein, A. Benselama, and M. M. Mahmoud, "Enhanced frequency regulation in renewable microgrids using a WSOA-based cascaded (1 + PDD 2) − (1 + ? ? I) controller and EV-assisted energy support," *Int. J. Robot. Control Syst.*, vol. 6, no. 3, pp. 2281–2303, 2026, https://doi.org/10.31763/ijrcs.v6i3.2679.

[7] M. Gad *et al.*, "Environmental DNA reveals drift-dominated microeukaryotic communities in Egypt's aquatic systems," *Euro-Mediterranean J. Environ. Integr.*, vol. 10, no. 4, pp. 3289–3300, 2025, https://doi.org/10.1007/s41207-025-00802-5.
[8] H. Mulam, V. P. Rameshkumaar, M. Bachute, and E. Muniyandy, "Dual attention holographic convolutional neural network based Ictal and Interictal States of automatic seizure detection using multi-channel scalp EEG with Humboldt squid optimization algorithm," *Smart Health*, vol. 37, p. 100599, 2025, https://doi.org/10.1016/j.smhl.2025.100599.
[9] M. H. Abdulameer *et al.*, "Potential application of BC2N monolayer as an anode for K-ion batteries: A theoretical study," *Comput. Theor. Chem.*, vol. 1252, p. 115374, 2025, https://doi.org/10.1016/j.comptc.2025.115374.
[10] M. H. Eid *et al.*, "Calcium modified mesoporous silica from marble for the removal of cadmium, lead, chromium, iron, and manganese from Siwa Oasis groundwater," *Sci. Rep.*, vol. 15, no. 1, p. 15802, 2025, https://doi.org/10.1038/s41598-025-15802-2.
[11] A. Almalkawi, A. Alsoboh, A. Amourah, and T. Sasa, "Estimates for the coefficients of subclasses defined by the q-Babalola convolution operator of bi-univalent functions subordinate to the q-Fibonacci analogue," *Eur. J. Pure Appl. Math.*, vol. 18, no. 3, pp. 100–115, 2025, https://doi.org/10.29020/nybg.ejpam.v18i3.6499.
[12] S. Ruttala, N. Jayaram, B. Kumar, and S. V. K. Naresh, "A comprehensive review of EV chargers: Topologies, standards, commercial implementations, and research challenges," *IEEE Access*, vol. 14, pp. 25623–25649, 2026, https://doi.org/10.1109/ACCESS.2026.3664945.
[13] R. Alika, E. M. Mellouli, and E. H. Tissir, "Adaptive cruise control of the autonomous vehicle based on sliding mode controller using Arduino and ultrasonic sensor," *J. Robot. Control*, vol. 5, no. 1, pp. 301–311, 2024, https://doi.org/10.18196/jrc.v5i1.20519.
[14] M. Elnady and S. Ozana, "Artificial intelligence techniques in Vehicle-to-Grid (V2G) systems: A review, comparative study, and model evaluation," *J. Energy Storage*, vol. 135, p. 118155, 2025, https://doi.org/10.1016/j.est.2025.118155.
[15] C. Vennila, S. Selvakumaran, K. Preetha, and G. Muralikrishnan, "Artificial intelligence-based adaptive control for vehicle-to-grid and grid-to-vehicle operations in electric vehicle charging stations," *Renew. Energy*, vol. 257, p. 124769, 2026, https://doi.org/10.1016/j.renene.2025.124769.
[16] D. Mazumdar, P. K. Biswas, C. Sain, and T. S. Ustun, "GAO optimized sliding mode based reconfigurable step size Pb&O MPPT controller with grid integrated EV charging station," *IEEE Access*, vol. 12, pp. 10608–10620, 2024, https://doi.org/10.1109/ACCESS.2023.3344275.
[17] F. Yu, Q. Yin, Z. Zhu, and X. Cheng, "A multienergy interface electric-drive-reconstructed onboard charger for EVs with integrated control strategy," *IEEE Trans. Power Electron.*, vol. 39, no. 4, pp. 4050–4061, 2024, https://doi.org/10.1109/TPEL.2023.3348822.
[18] A. Raj *et al.*, "Adaptive Q-wavelet transform and Kalman filtering for power quality disturbance prediction and carbon emission impact analysis in smart grids," *Eng. Reports*, vol. 8, no. 5, pp. 1–25, 2026, https://doi.org/10.1002/eng2.70825.
[19] W. F. Mbasso *et al.*, "EABIF for exploration-aware metaheuristic benchmarking and behavior-triggered control (CEC-2025)," *Appl. Soft Comput.*, vol. 199, p. 115344, 2026, https://doi.org/10.1016/j.asoc.2026.115344.
[20] A. Kodakkal, R. Veramalla, S. R. Salkuti, and L. D. Gottimukkula, "Optimized hybrid EV charging system interconnected with the grid," *World Electr. Veh. J.*, vol. 17, no. 3, p. 119, 2026, https://doi.org/10.3390/wevj17030119.
[21] V. R. Birudala, "Optimization of EV charging systems using hybrid GWO-PSO MPPT for PV source," *J. Eng. Technol. Ind. Appl.*, vol. 12, no. 58, pp. 1459–1465, 2026, https://doi.org/10.5935/jetia.v12i58.3410.
[22] H. Guentri, T. Alaoui, V. Blazek, and A. Dahbi, "Robust LQR control design for high efficiency battery supercapacitor hybrid storage systems," *Int. J. Robot. Control Syst.*, vol. 6, no. 2, pp. 1405–1425, 2026, https://doi.org/10.31763/ijrcs.v6i2.2154.
[23] H. Al-Sairfi, F. M. Alelaj, M. K. Alhamli, and M. Fadel, "Comparative numerical evaluation of feed-spacer geometries in reverse osmosis modules for enhanced water treatment sustainability," *Membranes*, vol. 16, no. 1, p. 265, 2026, https://doi.org/10.3390/membranes16010265.
[24] A. K. Tripathi *et al.*, "Integration of solar PV panels in electric vehicle charging infrastructure: Benefits, challenges, and environmental implications," *Energy Sci. Eng.*, vol. 13, no. 4, pp. 2135–2152, 2025, https://doi.org/10.1002/ese3.70014.
[25] H. S. Gohari, A. Safaeinasab, K. Abbaszadeh, P. Sergeant, and H. Vansompel, "Multiport buck-boost integrated on-board EV charger for multi-energy powertrains," *IEEE Access*, vol. 14, pp. 40478–40496, 2026, https://doi.org/10.1109/ACCESS.2026.3672173.
[26] J. Gupta, R. Maurya, and S. R. Arya, "Designing an on-board charger to efficiently charge multiple electric vehicles," *Chinese J. Electr. Eng.*, vol. 9, no. 2, pp. 38–56, 2023, https://doi.org/10.23919/CJEE.2023.000019.
[27] F. M. Alelaj *et al.*, "An offline digital-twin-assisted decision-support framework for dynamic RO under Kuwait solar-availability conditions," *Membranes*, vol. 16, no. 1, p. 281, 2026, https://doi.org/10.3390/membranes16010281.
[28] R. K. Lenka, A. K. Panda, and L. Senapati, "Grid integrated multifunctional EV charging infrastructure with improved power quality," *J. Energy Storage*, vol. 76, p. 109637, 2024, https://doi.org/10.1016/j.est.2023.109637.
[29] M. F. Elnaggar, M. M. Mahmoud, A. A. El-Rahman, and M. T. Mohamed, "WSA-tuned fractional TD–TI controller with vehicle-to-grid support for enhanced frequency regulation in renewable-based microgrids," *Sci. African*, vol. 34, p. e03622, 2026, https://doi.org/10.1016/j.sciaf.2026.e03622.

[30] H. Chaib, B. Belabbas, F. M. Alelaj, and A. Ma, "Adaptive smart energy management for wind-battery systems considering grid fault scenarios," *Bul. Ilm. Sarj. Tek. Elektro*, vol. 8, no. 4, pp. 1127–1147, 2026, https://doi.org/10.12928/biste.v8i4.16033.
[31] M. Tarek and M. I. M. Elzein, "Sustainable energy management in islanded microgrids via HHO – BE tuned adaptive controllers and demand-side flexibility," *Eng. Reports*, vol. 8, no. 1, pp. 1–20, 2026, https://doi.org/10.1002/eng2.70561.
[32] H. V. Nguyen, D. C. Lee, and F. Blaabjerg, "A novel SiC-based multifunctional onboard battery charger for plug-in electric vehicles," *IEEE Trans. Power Electron.*, vol. 36, no. 5, pp. 5635–5646, 2021, https://doi.org/10.1109/TPEL.2020.3026034.
[33] S. Vijayakumar and N. Sudhakar, "Golden eagle optimized fractional-order PI controller design for a PFC SEPIC converter in EV charging," *Sci. Rep.*, vol. 14, no. 1, p. 69653, 2024, https://doi.org/10.1038/s41598-024-69653-4.
[34] H. A. Brahmi *et al.*, "Robust Type-2 fuzzy logic control of dual-star induction motor-based electric vehicles for harsh mining environments," *Int. J. Robot. Control Syst.*, vol. 6, no. 3, pp. 2449–2473, 2026, https://doi.org/10.31763/ijrcs.v6i3.2801.
[35] M. T. Mohamed *et al.*, "Intelligent frequency regulation in islanded microgrids using a crayfish-tuned FO–(PD–PI) controller with energy storage coordination," *J. Low Freq. Noise Vib. Act. Control*, vol. 0, no. 0, pp. 1–32, 2026, https://doi.org/10.1177/14613484261429576.
[36] M. T. Mohamed *et al.*, "Delay-tolerant HHO-tuned fuzzy fractional controller for frequency regulation in renewable-powered microgrids with HFC integration," *J. Low Freq. Noise Vib. Act. Control*, vol. 0, no. 0, pp. 1–29, 2026, https://doi.org/10.1177/14613484261470210.
[37] B. S. Atia, F. M. Alelaj, M. M. Mahmoud, and A. Ma, "Crocodile optimizer-based DC chopper control for voltage dip and swell mitigation in PMSG-based WT," *Bul. Ilm. Sarj. Tek. Elektro*, vol. 8, no. 4, pp. 1087–1106, 2026, https://doi.org/10.12928/biste.v8i4.15464.
[38] F. Yu, Z. Zhu, X. Liu, and Z. Zhang, "Electric-drive-reconstructed onboard charger for solar-powered electric vehicles incorporating six-phase machine," *IEEE Trans. Power Electron.*, vol. 37, no. 6, pp. 6544–6555, 2022, https://doi.org/10.1109/TPEL.2022.3140410.
[39] V. Shah, G. Kumawat, and S. Payami, "Solar powered electric drive-train with integrated multifunctional dual power on-board charger incorporating N-phase SRM," in *Proc. 10th IEEE Int. Conf. Power Electron., Drives Energy Syst. (PEDES)*, 2022, https://doi.org/10.1109/PEDES56012.2022.10080481.
[40] A. Zar, H. Rehman, and I. Ahmad, "Neural network based optimized barrier conditioned double super-twisting sliding mode controller of electric vehicle charger with grid to vehicle and vehicle to grid modes," *J. Energy Storage*, vol. 74, p. 109234, 2023, https://doi.org/10.1016/j.est.2023.109234.
[41] S. Saleem, I. Ahmad, S. H. Ahmed, and A. Rehman, "Artificial intelligence based robust nonlinear controllers optimized by improved gray wolf optimization algorithm for plug-in hybrid electric vehicles in grid to vehicle applications," *J. Energy Storage*, vol. 75, p. 109332, 2024, https://doi.org/10.1016/j.est.2023.109332.
[42] V. R. Birudala *et al.*, "Bidirectional DC-DC converter for V2G and G2V using decoupled PI controller," in *Proc. 6th Int. Conf. Trends Material Sci. Inventive Materials (ICTMIM)*, pp. 655–659, 2026, https://doi.org/10.1109/ICTMIM68190.2026.11506629.
[43] D. Mishra, B. Singh, and B. K. Panigrahi, "Sigma-modified power control and parametric adaptation in a grid-integrated PV for EV charging architecture," *IEEE Trans. Energy Convers.*, vol. 37, no. 3, pp. 1965–1976, 2022, https://doi.org/10.1109/TEC.2022.3145884.
[44] S. J. Ríos, E. Sánchez-Gutiérrez, and S. Falcones, "High-efficiency bidirectional DC–DC converter control for PV-integrated EV charging stations: A real-time MBPC approach," *World Electr. Veh. J.*, vol. 17, no. 5, p. 229, 2026, https://doi.org/10.3390/wevj17050229.
[45] M. Fadel and H. Al Sairfi, "Adaptive fuzzy energy management of wind-battery systems with flexible desalination load," *Energy Sci. Eng.*, pp. 1–17, 2026, https://doi.org/10.1002/ese3.70570.
[46] S. Nadweh, I. M. Elzein, D. E. M. Wapet, and M. M. M. Benameur, "Optimizing control of single-ended primary inductor converter integrated with microinverter for PV systems: Imperialist competitive algorithm," *Energy Explor. Exploit.*, 2025, https://doi.org/10.1177/01445987251382002.
[47] P. Baltazar, J. D. Barros, and L. Gomes, "A distributed electric vehicles charging system powered by photovoltaic solar energy with enhanced voltage and frequency control in isolated microgrids," *Electronics*, vol. 15, no. 2, p. 418, 2026, https://doi.org/10.3390/electronics15020418.
[48] M. Basu *et al.*, "Flexible dynamic optimal power flow integrating renewable energy sources and electric vehicle parking IOT," *Eng. Reports*, vol. 7, no. 12, p. e70568, 2025, https://doi.org/10.1002/eng2.70568.
[49] M. K. Azeem, H. Armghan, Z. E. Huma, I. Ahmad, and M. Hassan, "Multistage adaptive nonlinear control of battery-ultracapacitor based plugin hybrid electric vehicles," *J. Energy Storage*, vol. 32, p. 101813, 2020, https://doi.org/10.1016/j.est.2020.101813.
[50] N. F. Ibrahim *et al.*, "Enhanced control of single-stage PV-STATCOM using hybrid MPPT and adaptive AHLMS for power quality improvement," *IEEE Access*, vol. 13, pp. 200253–200270, 2025, https://doi.org/10.1109/ACCESS.2025.3635707.
[51] S. Bagherwal and S. Mahapatra, "A robust sliding mode control strategy for DC voltage stabilization in solar powered electric vehicle charging station," *Int. J. Green Energy*, vol. 22, no. 2, pp. 432–448, 2025, https://doi.org/10.1080/15435075.2024.2415542.

[52] M. S. Priyadarshini *et al.*, "Microcontroller-based prototype model of a solar wireless electric vehicle-to-vehicle charging system with real-time battery voltage monitoring," *Bul. Ilm. Sarj. Tek. Elektro*, vol. 7, no. 3, pp. 527–540, 2025, https://doi.org/10.12928/biste.v7i3.13232.
[53] P. Sinha *et al.*, "Classifying power quality issues in railway electrification systems using a nonsubsampled contourlet transform approach," *Eng. Reports*, vol. 7, no. 8, p. e70301, 2025, https://doi.org/10.1002/eng2.70301.
[54] P. Vinay Kumar, "An ANFIS based grid connected renewable source bidirectional SEPIC converter multifunctional EV charger with reduced peak and disturbances," *J. Inf. Syst. Eng. Manag.*, vol. 10, no. 29s, pp. 1077–1089, 2025, https://doi.org/10.52783/jisem.v10i29s.4769.
[55] P. Sinha *et al.*, "Efficient automated detection of power quality disturbances using nonsubsampled contourlet transform & PCA-SVM," *Energy Explor. Exploit.*, vol. 00, no. 00, pp. 1–15, 2025, https://doi.org/10.1177/01445987241312755.
[56] G. Kumar and B. Singh, "PV integrated single-stage isolated PFC charger for solar panel installed LEV," *IEEE Trans. Consum. Electron.*, vol. 71, no. 4, pp. 9796–9807, 2025, https://doi.org/10.1109/TCE.2025.3602298.
[57] P. Singla *et al.*, "Design and simulation of 4 kW solar power-based hybrid EV charging station," *Sci. Rep.*, vol. 14, no. 1, p. 56833, 2024, https://doi.org/10.1038/s41598-024-56833-5.
[58] B. Benbouya *et al.*, "Dynamic assessment and control of a dual star induction machine state dedicated to an electric vehicle under short-circuit defect," *Int. J. Robot. Control Syst.*, vol. 4, no. 4, pp. 1731–1745, 2024, https://doi.org/10.31763/ijrcs.v4i4.1557.
[59] R. Moumni *et al.*, "Comparative study of electric vehicle propulsion systems using field-oriented controlled dual PMSMs with novel control strategies based on an EPS filter and a fuzzy logic regulator for enhanced stability and safety," *Energy Sci. Eng.*, pp. 1–18, 2026, https://doi.org/10.1002/ese3.70582.
[60] M. M. Hussein *et al.*, "Regulation of multi-area power system load frequency in presence of V2G scheme," *PLoS One*, vol. 18, no. 9, p. e0291463, 2023, https://doi.org/10.1371/journal.pone.0291463.
[61] K. Srivastava, S. Kumar, and R. Maurya, "A robust BCNMCC based variance smoothing approach for SPV based grid integrated EV battery charging system," *J. Energy Storage*, vol. 72, p. 108361, 2023, https://doi.org/10.1016/j.est.2023.108361.
[62] R. Moumni, K. Laroussi, I. Benlaloui, M. M. Mahmoud, and M. F. Elnaggar, "Optimizing single-inverter electric differential system for electric vehicle propulsion applications," *Int. J. Robot. Control Syst.*, vol. 4, no. 4, pp. 1772–1793, 2024, https://doi.org/10.31763/ijrcs.v4i4.1542.
[63] A. Keerthi and C. Dhanamjayulu, "A thorough review of energy management and an advanced control techniques for bi-directional DC-DC converters in electric vehicle applications," *Results Eng.*, vol. 27, p. 106726, 2025, https://doi.org/10.1016/j.rineng.2025.106726.
[64] S. Kumar, K. Srivastava, and T. Upadhyay, "STC–DAB converter integrated solar PV off-board charger for electric vehicles with power quality improvement," *IEEE Trans. Aerosp. Electron. Syst.*, vol. 61, no. 6, pp. 17500–17511, 2025, https://doi.org/10.1109/TAES.2025.3606428.
[65] S. Heroual *et al.*, "Comparative metaheuristic optimization of PI controllers for electric vehicle speed control," *Eng. Reports*, vol. 8, no. 6, p. e70875, 2026, https://doi.org/10.1002/eng2.70875.
[66] R. Kassem *et al.*, "Enhanced multiphase interleaved boost converter interface for grid-connected PV power system," *IEEE Access*, vol. 12, pp. 151940–151954, 2024, https://doi.org/10.1109/ACCESS.2024.3469540.
[67] D. Selvaraj and D. Rangasamy, "Electric vehicle charging using roof top photovoltaic controlled with new hybrid optimization technique," *Indones. J. Electr. Eng. Comput. Sci.*, vol. 26, no. 3, pp. 1227–1234, 2022, https://doi.org/10.11591/ijeecs.v26.i3.pp1227-1234.
[68] H. Saleeb *et al.*, "Highly efficient isolated multiport bidirectional DC/DC converter for PV applications," *IEEE Access*, vol. 12, pp. 112000–112015, 2024, https://doi.org/10.1109/ACCESS.2024.3442711.
[69] F. Menzri *et al.*, "Applications of novel combined controllers for optimizing grid-connected hybrid renewable energy systems," *Sustainability*, vol. 16, no. 16, p. 6825, 2024, https://doi.org/10.3390/su16166825.
[70] H. Wei *et al.*, "Design and validation of a battery management system for solar-assisted electric vehicles," *J. Power Sources*, vol. 513, p. 230531, 2021, https://doi.org/10.1016/j.jpowsour.2021.230531.
[71] N. Shetty, "Electric vehicle charging with battery scheduling and multicriteria optimization using genetic algorithm," *J. Electr. Eng. Autom.*, vol. 2, no. 3, pp. 123–128, 2021, https://doi.org/10.36548/jeea.2020.3.003.
[72] T. Chen *et al.*, "An optimal control algorithm with reduced DC-bus current fluctuation for multiple charging modes of electric vehicle charging station," *World Electr. Veh. J.*, vol. 12, no. 3, p. 107, 2021, https://doi.org/10.3390/wevj12030107.
[73] M. I. B. M. Mawardi, N. H. N. Ali, N. M. Hidayat, E. Abdullah, M. Umair, and M. A. T. M. Yusoh, "Solar-based electric vehicle charging with bidirectional buck-boost converter and proportional-integral control algorithm," *J. Sustain. Dev. Energy, Water Environ. Syst.*, vol. 14, no. 1, p. 130637, 2026, https://doi.org/10.13044/j.sdewes.d13.0637.
[74] N. Benalia *et al.*, "Enhancing electric vehicle charging performance through series-series topology resonance-coupled wireless power transfer," *PLoS One*, vol. 19, no. 3, p. e0300550, 2024, https://doi.org/10.1371/journal.pone.0300550.
[75] Z. Zhang, Y. Guo, and X. Song, "Improved nonlinear extended state observer-based sliding-mode rotary control for the rotation system of a hydraulic roofbolter," *Entropy*, vol. 24, no. 1, p. 41, 2022, https://doi.org/10.3390/e24010041.
[76] T. Ivanovski, M. Brkić Bakarić, and M. Matetić, "Recent advances in metaheuristic algorithms," *Algorithms*, vol. 19, no. 1, p. 19, 2026, https://doi.org/10.3390/a19010019.

[77] S. Heroual *et al.*, "Genetic algorithm tuned controllers for high-performance indirect field-oriented control in DFIG-based WECS," *Bul. Ilm. Sarj. Tek. Elektro*, vol. 8, no. 1, pp. 294–310, 2026, https://doi.org/10.12928/biste.v8i1.15529.